Title
Tests of a Model Pole Assembly for the ALS U5.0 Undulator

Authors
Hassenzahl, W.V.
Hoyer, E.
Savoy, R.

Publication Date
1991-06-01

LBL-30938
UC-400

Lawrence Berkeley Laboratory
UNIVERSITY OF CALIFORNIA

Accelerator & Fusion Research Division

Tests of a Model Pole Assembly for the ALS U5.0 Undulator

W.V. Hassenzahl, E. Hoyer, and R. Savoy

June 1991

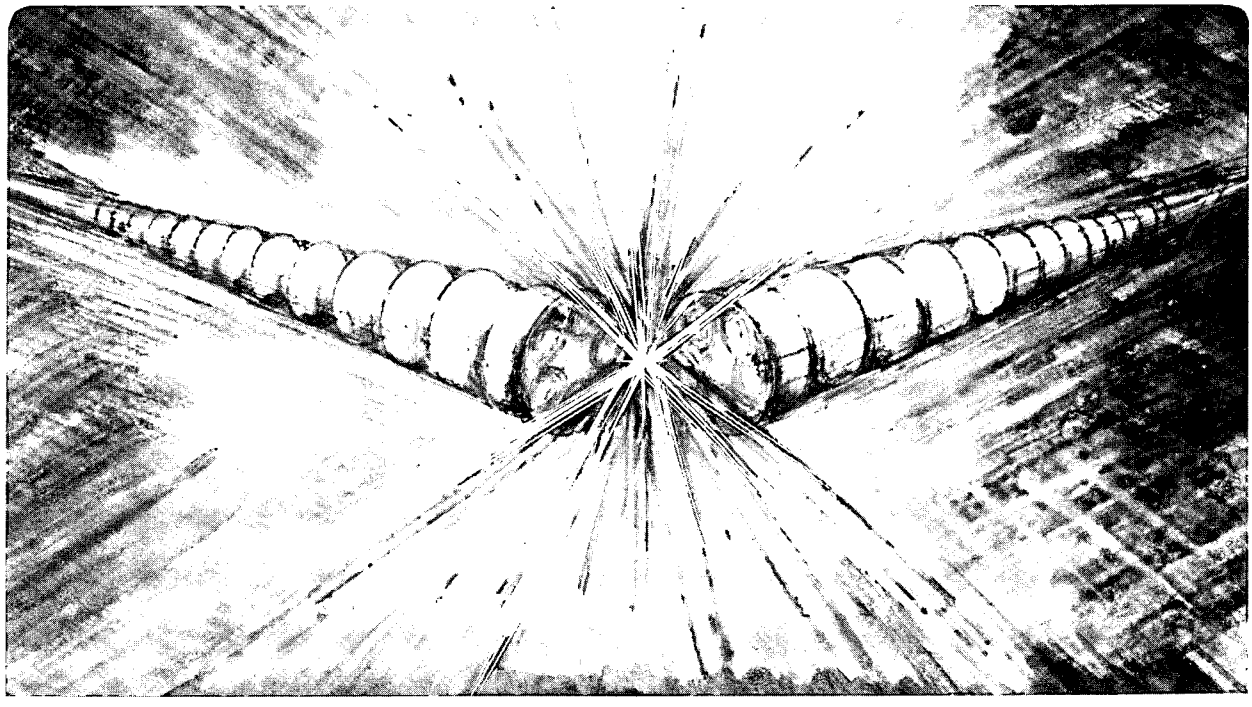

Prepared for the U.S. Department of Energy under Contract Number DE-AC03-76SF00098

DISCLAIMER

LBL-30938

TESTS OF A MODEL POLE ASSEMBLY FOR THE ALS U5.0 UNDULATOR*

W.V. Hassenzahl & E. Hoyer

Advanced Light Source
Accelerator and Fusion Research Division
Lawrence Berkeley Laboratory
1 Cyclotron Road
Berkeley, CA 94720

R. Savoy

Advanced Photon Source
Argonne National Laboratory
9700 South Cass Avenue
Argonne, IL 60439

June 1991

*This work was supported by the Director, Office of Energy Research, Office of Basic Energy Sciences, Materials Sciences Division of the U.S. Department of Energy, under Contract No. DE-AC03-76SF00098

Tests of a Model Pole Assembly for the ALS U5.0 Undulator

W. V. Hassenzahl and E. Hoyer - LBL and R. Savoy - ANL

ABSTRACT

The ALS insertion devices must meet very tight requirements in terms of field quality and field strength. Even though the ability to calculate the performance of a hybrid insertion device has improved considerably over the past few years, a model pole was assembled to test the ALS U5.0 undulator geometry and to verify the calculations. The model pole consists of a half period of the periodic structure of the insertion device with mirror plates at the midplane and at the zero-field, half-period planes. A Hall probe was used to measure the vertical component of the field near the midplane of the model as a function of gap and transverse position. Because of the tight field quality requirements the ALS insertion devices are designed to permit several types of correction, including the capability of adding magnetic material or iron at several locations to boost or buck the field. This correction capability was evaluated during our tests. The model is described and details of the test results are discussed, including the fact that the measured peak field is several percent higher than the calculated value, which is based on the measured magnetization of the blocks used in the model.

I. Introduction

Insertion devices for the Lawrence Berkeley Laboratory (LBL) Advanced Light Source (ALS) and other third generation synchrotron light sources must meet more stringent tolerance requirements than insertion devices built to date for existing light sources[1]. Considerable effort has been dedicated to the development of requirements for the U5.0 undulator, which has a 5 cm period[2] and will be the first insertion device for the ALS. The design choice for high performance devices is a hybrid configuration with vanadium permendur poles and neodymium-iron-boron (Nd-Fe-B) permanent magnets. The performance of a device is determined by the peak field at minimum gap and the magnetic field errors. The importance of these characteristics is discussed in reference 2. The peak field as a function of gap can be calculated with a three dimensional theory of hybrid devices[3]. An extension of this theory[4] was used to estimate the field errors due to various material and assembly tolerances in the U5.0 insertion device. This paper addresses the peak field characteristics.

Calculations of the magnitude of the magnetic field in insertion devices have been found to be accurate to a few percent, which has been confirmed with calculations of the field for the beam line 10 (BLX) device at SSRL and for the TOK at NSLS by several approaches[5,6]. (Note that the peak field on axis of high performance devices is not a strong function of pole height. For example, increasing the U5.0 pole height from 6.0 to 8.0 cm while keeping other factors constant results in a field increase of only 5%.) Even though this calculational capability exists, a half period model of the magnetic structure was

constructed and tested to ensure peak field performance of the U5.0 undulator. This model pole assembly is shown in Fig. 1. The coordinate system used in this report is that typically used for insertion device analysis. The major field component, B_y, is measured here; the electrons pass through the device in the z direction, and oscillate in the x direction. The transverse scans described in this report are in the x direction.

The U5.0 model was thoroughly tested to determine the peak field at the midplane and the transverse variation of the vertical field for the nominal design configuration, for half excitation (i.e., using only half of the magnet blocks), and for zero excitation (no magnets). These runs allowed an estimation of the effects of saturation and remanent fields in the vanadium permendur poles. Initial tests confirmed that the peak vertical field was greater than the 0.88 T calculated for a half gap of 7 mm.

Because it may be necessary to tune the fields to meet accelerator or spectral requirements, one method of adjusting the magnetic field in ALS insertion devices was designed into the model. It consists of placing iron or permanent magnet inserts on the sides of the poles between the overhanging permanent magnet material. These inserts have two effects on the fields. First, they either boost or reduce the potential of the poles, and second, depending on the distance of the material from the midplane, they also cause a transverse redistribution of the field.

This report describes in detail the model pole and the set of measurements made on it. It includes the following:

A description of the model pole.
A presentation of peak field at the midplane as a function of gap.
A description of the effects of decreasing the excitation.
A discussion of the field variations due to various inserts.
A description of the transverse variation in the vertical field due to side inserts.

The lists of planned and actual tests on the U5.0 Model pole including references to filenames for the data are summarized in ALS beamline report xxxxx.

II. Description of the U5.0 Model Pole Assembly

The U5.0 model pole assembly is shown in Figs. 1 to 5. It consists of: 1. a vanadium permendur pole; 2. eight Nd-Fe-B blocks that are 0.85 cm thick, half the thickness of the U5.0 blocks; 3. a keeper that holds the pole and blocks in place and allows iron and permanent magnet material, sometimes called current (or charge) sheet equivalent material (CSEM) inserts or studs to be placed close to the pole ; 4. a set of three mirror plates that define the magnetic symmetry of the device (one is at the midplane and one at

each of the +/- 1/4 period planes); and 5. a mounting fixture, which simulates the backing beam - including the side pieces. This fixture allows the pole to be positioned at distances above the midplane corresponding to various half gaps.

The pole and the eight CSEM blocks form half of a U5.0 half period, which is the smallest unit of the periodic magnetic structure that can be modeled in this way. Note that the blocks are made from left over Beamline 10 blocks that were cut and ground to the proper dimensions for this test. Each of these blocks was half the thickness of a U5.0 block, 1.5 times the width and is of the correct height. Because they were cut out of larger blocks in which the easy axis orientation was not completely uniform, they did not necessarily retain the magnetic moment orientation of the original BLX blocks, and may have larger transverse moments than the original blocks. The characteristics of the blocks are given in Table I.

TABLE I

Characteristics of the blocks used for the U5.0 model pole. The A and B refer to the two U5.0 model pole blocks made from the Beamline 10 block designated by the 9xx. Block 50B912 was measured several times to monitor system reproducibility, which was about +/- 25 Gauss. The moments have not been corrected for temperature variation.

Number	Mz (Gauss)	Mx (Gauss)	My (Gauss)
50B912	11418	-166	-376
50A912	11392	-294	371
50A914	11429	-272	610
50B914	11412	-199	-493
50A932	11420	81	-425
50B932	11417	222	411
50A935	11364	221	413
50B935	11404	79	-406
50A929	11361	-96	-371
50B929	11386	-229	430
50B912	11385	-158	-364

The top piece of the mounting fixture is positioned a distance above the pole to simulate the position of the iron backing beam in the U5.0 geometry. The pole assembly is shown in Fig. 2, a cut away view, which shows a track at the bottom to allow the Hall probe to be positioned under the pole.

The probe can be moved in the x direction from one side of the assembly to the other. The position of the active component of the probe is about 1.0 mm above the midplane. This offset requires the measured fields B_m to be corrected, using the relationship

$$B_o = B_m [\cosh(2\pi\Delta y/\lambda_u)]^{-1} = 0.992\, B_m ,$$

to obtain the field B_o at the midplane, where λ_u is the 5 cm period length.

The aluminum pole keeper shown in Fig. 3 has three tapped holes on each side that can hold iron or CSEM inserts. These inserts were all 5.6 mm (0.220") in diameter and were held in threaded brass rods, which could be used to accurately position the inserts close to the vanadium permendur pole. The characteristics of the inserts are listed below in Table II.

Table II

The lengths and types of inserts used for the U5.0 model pole. All inserts were 5.6 mm in diameter.

Insert Type	Length (mm)	Polarity
Iron	11.2	N/A
Iron	20.6	N/A
CSEM	11.2	+ and -
CSEM	20.6	+ and -

III. The gap dependence of the magnetic field

The peak field was measured at several gaps. This field is the algebraic sum of all the spatial harmonics.

$$B_p = \sum_{i=0}^{\infty} B_{2i+1}$$

The quantity of interest, however, is the effective field, B_{eff}, which enters into the calculation of the spectrum of the light emitted by the undulator. B_{eff} is given by

$$B_{eff} = \left\{ \sum_{i=0}^{\infty} [B_{2i+1}/(2i+1)]^2 \right\}^{1/2}$$

The relationship between the peak field and the effective field depends on the geometry of the device and can be found from the spatial field distribution, i.e., the magnitude of the spatial harmonics. The gap dependence of each spatial harmonic of the field is given by

$$B2i+1(g1) = B2i+1(g2)\exp(2\pi\{2i+1\}[g2-g1]/\lambda_u).$$

The spatial field distribution can be calculated accurately by POISSON using geometry and measured permeability of the pole. The theory of hybrid insertion devices developed by K. Halbach[4] can then be combined with these POISSON results to predict the peak field.

Precise ceramic gauge blocks (ground to a tolerance of 5μm) were used to set accurately the half gap of the model pole to 7, 10 and 20mm. These gauge blocks also prevented pole tilt. The half gap was adjusted to intermediate values by using a precision depth gauge to measure the distance from the top of the side plates to the top of the backing beam. At each fixed gap, the Hall probe was scanned in the transverse x direction and the field at the center (x=0, z=0) of the model was recorded.

The gap dependence of the peak field is given in Table III and in Figs. 6 and 7. The results of the field calculations are included in Tables IV and V (attached), which were produced with an application program[7] we developed using the Excel spreadsheet. This program permits a quick and convenient application of Halbach's theory.

TABLE III

Measurements of peak field with different excitation levels

Half Gap (mm)	Full Excitation (T)	Half Excitation (T)	Zero Excitation (T)
4.24		1.1817	
7.00	1.0291	.7337	0.00043
8.00		.6291	
9.00		.5311	
9.88	.6736		
10.00	.6593	.4593	0.00041
15.00	.3368		
20.00	.1748	.1236	0.00048
30.00	.0499		
40.00	.0144		
50.00	.0043		

The calculated fields are slightly smaller than the measured values. This difference varies from about 3% for the smallest gap to 10% for the largest gap. The source of this discrepancy is not understood at this time. Fortunately, the measured fields are larger. At a 7.0 mm half gap the measured peak field is 1.03 T, which yields an effective field of about 0.96T, which is well above the design goal of 0.88 T. for the U5.0 Undulator.

The magnitude of the peak field depends on the scalar potential (level of excitation) of the pole. The distribution depends only on the geometry and level of saturation of the pole. Thus, for a given gap, the ratio of any spatial field harmonic to the fundamental will be independent of pole excitation (ignoring saturation and remanent field effects).

The peak fields were also measured when the pole was energized by only half of the permanent magnet material (the top layer of permanent magnet blocks was removed) and when all CSEM was removed. This data is given in Table III and Fig. 8. The field as a function of gap can be described by the same exponential behavior, but with different coefficients. However, the field values are about 70% of those for the full excitation. This relatively large percentage is due to CSEM overhang and pole saturation.

IV. Magnetic Field variation in the x direction

Transverse (x) profiles of B_y were obtained by scanning the Hall probe from the field-free region on one side of the pole, $x \approx +100$ mm, to an equivalent position on the other side, $x \approx -100$ mm. The field was measured at discrete locations (usually every 2 mm) along the x path of the Hall probe through the model. The x positioning accuracy was about ±0.25mm. The output of the Bell Gaussmeter was measured with a digital voltmeter and typed into a spreadsheet, which allowed us to plot the data immediately. This feature provided a quick check for typing errors and a simple analysis of the data on the spot. These results were used to plan subsequent measurements.

Figure 9 is a transverse scan for a 7 mm half gap with full pole excitation. The field under the pole is relatively flat from -20 mm to +20 mm. The magnetic field decreases as the edge of the pole is approached. At the edge of the pole (±40 mm from the pole center) the field has dropped to about 75% of the central value. The magnetic field approaches zero at ±90 mm from the pole center.

The repeatability of the field measurements is quite good even though the Hall probe was manually positioned. The difference between two consecutive, presumably identical field measurements is shown in Fig. 10. In the central 50 mm the repeatability is about ±0.05%. The maximum difference in field readings was about 1% of the central field and occurred in the region of strong field gradient at the edge of the pole.

The field distribution near the center of the device affects the spectral performance of the insertion devices and the operation of the storage ring. Figures 11 and 12 show the normalized magnetic field near the center of the device for half gaps of 7, 10, 15 and 20 mm on different scales. The field is expected to be more uniform than it appears at the magnification shown in Fig. 12. However, all the measurements in Fig. 12 contain a tiny field component that is nearly proportional to the absolute value of the distance from the center. We estimate that the magnitude of this component is about 0.2 % of the peak field at the center and falls off to zero at about ±10mm. The apparent reason for this unexpected field profile is the tapped holes for the two screws that were used to hold the aluminum track to the bottom mirror plate (See Fig. 1, which shows five pairs of screws that are used to mount the aluminum track to the mirror plate). Unfortunately one pair of screws is precisely at the transverse center of the model. The screws were tested and found not to be very magnetic so we do not expect their presence to cause the observed effect. However, the absence of ferromagnetic material within the mirror plate (the screw holes) means that it is magnetically deficient. To analyze the effect of the holes we can represent them by magnetic charges[4]. These charges would increase the magnetic field nearby, in particular at x = z = 0.0, and produce the observed variation in the field profile. Also, the same model structure (with a new mirror plate) will be used to test a scaled model of the next ALS insertion device, the U8.0 Undulator, where we hope to see a flatter distribution and thus verify this effect.

Figure 13 shows the differences between the normalized (subscript n) field values for different half gaps ($B_{yn}(7)$-$B_{yn}(10)$, $B_{yn}(7)$-$B_{yn}(15)$, $B_{yn}(7)$-$B_{yn}(20)$) as a function of transverse position x. The graph shows that the larger the half gap the faster the fields fall off across the pole, whereas they decrease more slowly outside the pole. The left-right asymmetry is apparently an indication of a slight pole tilt.

V. Field modifications due to "shims"

A major concern in the design of an insertion device is that the magnitude and/or distribution of the error fields exceeds the specifications. The underlying philosophy in ALS insertion device design is to limit errors by assigning tight tolerances. But, as a fallback position, the ALS insertion device design includes several methods of local field correction. We used the U5.0 model pole assembly to evaluate two methods of adjusting the field; either CSEM or iron inserts were placed on the sides of the pole. Because of the model geometry, i.e. there are mirror planes at the quarter period points, the effect of any pole modification is the same as if all poles had received the same relative change in scalar potential. It is the same as adding inserts to each pole in the periodic structure.

The CSEM inserts were magnetized along the length (or axis) of the cylinder, and the CSEM could be oriented to either boost or reduce the central magnetic field (and the potential of the pole). The iron inserts affected the capacitance of the pole and led to a reduction in central field.

Field measurements with inserts in place were analyzed as field difference maps, which were developed via the following procedure. First, a gap was set and a transverse scan was recorded without inserts to establish a baseline. Second, an insert was selected and installed on one side of the model and another scan was recorded. Third, an insert was installed on the other side of the pole and a scan was made. Fourth, the first insert was removed from the model and a scan was made. Fifth, the second insert was removed and another baseline scan was made. The first and the last baseline scan were compared for changes and to determine repeatability.

The three difference maps were obtained by subtracting the field with inserts from the average of the baseline scans. These curves were then normalized to the peak field in the baseline runs. Data will be described in the next section.

VI. Effect of CSEM inserts on the lateral field distribution

Two typical difference maps, with one and two CSEM inserts in the bottom position , are shown in Fig. 14. The pair of inserts boosted the field under the pole by about 0.35%. The large field excursions at about ±60 mm are caused by flux that goes directly from the "magnetic charge" at the end of the insert to the midplane, which is a graphic example of the direct field[4]. The field in the center of the device is boosted twice as much for two inserts as it is for one; within the accuracy of the measurements the inserts obey the superposition law. This suggests that saturation does not degrade the effect of the inserts.

The change of center field as a function of the distance of the CSEM insert from the pole was also studied. The results are plotted in Fig. 15. One turn of the screw that captures the CSEM insert increases the distance from the pole by 1.81 mm. The figure shows that 50% of the effect occurs within the first two turns of the screw.

A drawback of most correction schemes is that they are gap dependent, making it possible to shim the device at one specific gap perfectly, but often by reducing the performance of the device at other gaps. Therefore, we studied the effect on the center field of long CSEM insert in the bottom and middle position as a function of half gap. The results of these measurements are shown in Fig. 16. The ordinate is the logarithm (base e) of the normalized field values Bh/B7 for the central field without inserts and the normalized field variation $\Delta B_h/\Delta B7$ for the effect of the inserts. $\Delta B7$ is the field change at the center of the device for a half gap of 7 mm due to a pair of inserts. The abcissa is the half gap.

Except for small gaps, the field produced by the inserts tracks that produced by the main CSEM. Our suspicion is that these differences are caused by saturation effects in the pole. There is a significant

variation in the normalized change of the central field and the field difference from a 0.7 cm gap to a 1.0 cm gap. Even though the model does not simulate the effect of a change in only one pole, it gives a good indication of the usefulness of this approach for error control. This suggests that a correction valid at 0.7 cm would be about twice as strong as necessary at gaps of 1.0 cm and greater.

VII. Effect of iron inserts on the lateral field distribution

The effect of iron inserts on the transverse field distribution was also studied. Figure 17 shows the result of a scan with an insert on the left side. The large peak at -50 mm is caused by the direct fields of the insert. The field change under the pole is not constant but shows an gradient. The gradient suggests that there is a vector potential drop along the pole, which is a sign of pole saturation. Figure 18 shows the field distribution for an insert on the right hand side on the pole, clearly identifiable by the large peak at about +50 mm. The gradient across the gap is now in the reverse direction.

The change in field distribution for a pole with an insert on each side is plotted in Fig. 19. The signature of the inserts are the large peaks to the left and right of the pole. The field change under the pole is now constant. If we add the two scans with one insert on either side of the pole and compare the result with the measurement with both inserts on the pole we find that the two curves are identical.

Finally, we studied the effect of pairs of inserts at various heights on the transverse field distribution. The results are shown in Fig. 20. The case where the inserts are in the bottom position is marked by the diamonds and is the same curve as in Fig. 19. This curve is shown for reference. The field change under the pole for the inserts in the middle and top position is nearly independent of the insert pair height. Note that there are practically no direct fields in the midplane for the inserts in the higher positions as evidenced in the lack of peaks beyond the edge of the poles.

VIII. References:

1. A. M. Fauchet, B. C. Craft, J. N. Galayda, H. Hsieh, A. Luccio, J. B. Murphy, C. Pellegrini, A. van Steenbergen, G.Vignola, L. H. Yu, R. R. Freeman, and B. M. Kincaid, "Beamline U13-TOK", Brookhaven National Laboratory Annual Reports 1985 and 1986.

2. "U5.0 Undulator Conceptual Design Report", LBL Report, PUB-5256, November 1989.

3. K. Halbach, "Design of Magnets", Jülich videotape lecture series, May to June, 1985

4. K. Halbach,"Design of hybrid insertion devices", LBL lecture series, October, 1988 to March 1989

5. B. M. Kincaid, "Analysis of Field Errors in Existing Undulators" NIM Vol. A291, Nos. 1,2 May 20, 1990.

6. Private communication, D Humphries, LBL.

7. To be published SSRL experience with model.

8. R.Savoy, to be published

Table IV

Analysis of U5.0	8/15/90 13:46	U5.0 h=7mm	U5.0 h=8mm	U5.0 h=10mm	U5.0 h=15mm
Variables:					
Pole height	D3pole	6.00 cm	6.00 cm	6.00 cm	6.00 cm
Overhang side	(Overside	1.25 cm	1.25 cm	1.25 cm	1.25 cm
Overhang top	(Overtop	1.20 cm	1.20 cm	1.20 cm	1.20 cm
Results					
Field Bo	Bmax	**9883.5 G**	**8310.1 G**	**6113.8 G**	**3083.4 G**
Operating Point of the CSEM	Opoint	0.837	0.843	0.850	0.858
CSEM Volume	csemvolume	44582 ccm	44582 ccm	44582 ccm	44582 ccm
CSEM Price per ccm	csempriceccm	2.50$	2.50$	2.50$	2.50$
CSEM Price Total	csempricetot	**111455$**	**111455$**	**111455$**	**111455$**
Fixed Geometry Data					
Period length Lambda	lambda	5.00 cm	5.00 cm	5.00 cm	5.00 cm
Number of Periods	Nperiods	89.20	89.20	89.20	89.20
Half thickness Pole (longitudinal)	D: polethickness	0.40 cm	0.40 cm	0.40 cm	0.40 cm
Half thickness CSEM (longitudinal)	H: csemthickness	0.85 cm	0.85 cm	0.85 cm	0.85 cm
Dimensional check		OK	OK	OK	OK
Full lateral pole width (in x direction)	2D1 polewidth	8.00	8.00	8.00	8.00
Register distance	I registerheight	0.20	0.20	0.20	0.20
Material Data					
Remanent field of CSEM Br in Gauss	Br	12011 G	12011 G	12011 G	12011 G
Coercive Field of CSEM Hc in Oersted	Hc	11250 Oe	11250 Oe	11250 Oe	11250 Oe
Permeability of CSEM	mue	1.070	1.070	1.070	1.070
Input from 2D calculations					
Halfgap	h	0.70 cm	0.80 cm	1.00 cm	1.50 cm
D4 bad theoretical approximation		0.794	0.942	1.285	2.560
D4 from POISSON or equiv. code	D4 d4poisson	0.810	0.970	1.330	2.660
Excess Flux Coefficients (E.F.C.):					
Calculated by 2D-Code					
E.F.C. into pole face and side	ep+es	1.073	1.000	0.907	0.816
Calculated analytically					
E.F.C. into top of pole Et	et	0.824	0.824	0.824	0.824
E.F.C. into corner Ec≈0.5	ec	0.500	0.500	0.500	0.500
Analytical Flux coefficients					
Flux into top E01:	AFCe01	0.645	0.645	0.645	0.645
Flux into lateral side E03:	AFCe03	0.656	0.656	0.656	0.656
Flux and Capacitance calculations					
2D-Computer Results used as input					
Run #2: Scalar Potential of Pole	run2_v0	7383.46	8195.25	9806.79	13812.8
Run #2: Vector potential	run2_A	10000	10000	10000	10000
Run #3: Scalar Potential of Pole	run3_v0	119.52	131.8	154.33	202.13
Run #3: Scalar pot. Difference A30-A31	run3_A	301.51	322.21	358.77	425.92
Results					
Total Flux entering one pole (Gauss*sq.cm.)	Fluxtot	687615	687615	687615	687615
Integral of complex potential G0	IG0	0.824	0.824	0.824	0.824
Capacitance C2	cap_c2	171.78 cm	170.61 cm	169.13 cm	167.67 cm
Capacitance CF (Pole-Midplane)	cap_cf	21.67 cm	19.52 cm	16.32 cm	11.58 cm
Capacitance Cs (Pole-Side)	cap_cs	12.61 cm	12.22 cm	11.62 cm	10.54 cm
Capacitance C1 (Pole to adjacent pole)	cap_c1	34.37 cm	34.72 cm	35.30 cm	36.39 cm

Roland Savoy, M.S. 2-400, Lawrence Berkeley Laboratory, Berkeley CA 94720, Phone USA-(415)-486 5963 V9/8

Table V

Analysis of U5.0	8/15/90 13:47	U5.0 h=20mm	U5.0 h=30mm	U5.0 h=40mm	U5.0 h=50mm
Variables:					
Pole height	D3pole	6.00 cm	6.00 cm	6.00 cm	6.00 cm
Overhang side	(Overside	1.25 cm	1.25 cm	1.25 cm	1.25 cm
Overhang top	(Overtop	1.20 cm	1.20 cm	1.20 cm	1.20 cm
Results					
Field Bo	Bmax	**1615.2 G**	**457.1 G**	**130.1 G**	**37.1 G**
Operating Point of the CSEM	Opoint	0.860	0.860	0.861	0.861
CSEM Volume	csemvolume	44582 ccm	44582 ccm	44582 ccm	44582 ccm
CSEM Price per ccm	csempriceccm	2.50$	2.50$	2.50$	2.50$
CSEM Price Total	csempricetot	**111455$**	**111455$**	**111455$**	**111455$**
Fixed Geometry Data					
Period length Lambda	lambda	5.00 cm	5.00 cm	5.00 cm	5.00 cm
Number of Periods	Nperiods	89.20	89.20	89.20	89.20
Half thickness Pole (longitudinal)	D: polethickness	0.40 cm	0.40 cm	0.40 cm	0.40 cm
Half thickness CSEM (longitudinal)	H: csemthickness	0.85 cm	0.85 cm	0.85 cm	0.85 cm
Dimensional check		OK	OK	OK	OK
Full lateral pole width (in x direction)	2D1 polewidth	8.00	8.00	8.00	8.00
Register distance	I registerheight	0.20	0.20	0.20	0.20
Material Data					
Remanent field of CSEM Br in Gauss	Br	12011 G	12011 G	12011 G	12011 G
Coercive Field of CSEM Hc in Oersted	Hc	11250 Oe	11250 Oe	11250 Oe	11250 Oe
Permeability of CSEM	mue	1.070	1.070	1.070	1.070
Input from 2D calculations					
Halfgap	h	2.00 cm	3.00 cm	4.00 cm	5.00 cm
D4 bad theoretical approximation		4.880	17.250	60.638	213.065
D4 from POISSON or equiv. code	D4 d4poisson	5.090	18.000	63.240	222.060
Excess Flux Coefficients (E.F.C.):					
Calculated by 2D-Code					
E.F.C. into pole face and side	ep+es	0.791	0.783	0.782	0.782
Calculated analytically					
E.F.C. into top of pole Et	et	0.824	0.824	0.824	0.824
E.F.C. into corner Ec≈0.5	ec	0.500	0.500	0.500	0.500
Analytical Flux coefficients					
Flux into top E01:	AFCe01	0.645	0.645	0.645	0.645
Flux into lateral side E03:	AFCe03	0.656	0.656	0.656	0.656
Flux and Capacitance calculations					
2D-Computer Results used as input					
Run #2: Scalar Potential of Pole	run2_v0	17813.27	25813.28	33813.29	41813.17
Run #2: Vector potential	run2_A	10000	10000	10000	10000
Run #3: Scalar Potential of Pole	run3_v0	241.27	303.1	350.73	388.92
Run #3: Scalar pot. Difference A30-A31	run3_A	473.67	537.13	579.14	608.47
Results					
Total Flux entering one pole (Gauss*sq.cm.)	Fluxtot	687615	687615	687615	687615
Integral of complex potential G0	IG0	0.824	0.824	0.824	0.824
Capacitance C2	cap_c2	167.27 cm	167.14 cm	167.13 cm	167.13 cm
Capacitance CF (Pole-Midplane)	cap_cf	8.98 cm	6.20 cm	4.73 cm	3.83 cm
Capacitance Cs (Pole-Side)	cap_cs	9.82 cm	8.86 cm	8.26 cm	7.82 cm
Capacitance C1 (Pole to adjacent pole)	cap_c1	37.12 cm	38.02 cm	38.53 cm	38.87 cm

Roland Savoy, M.S. 2-400, Lawrence Berkeley Laboratory, Berkeley CA 94720, Phone USA-(415)-486 5963 V9/8

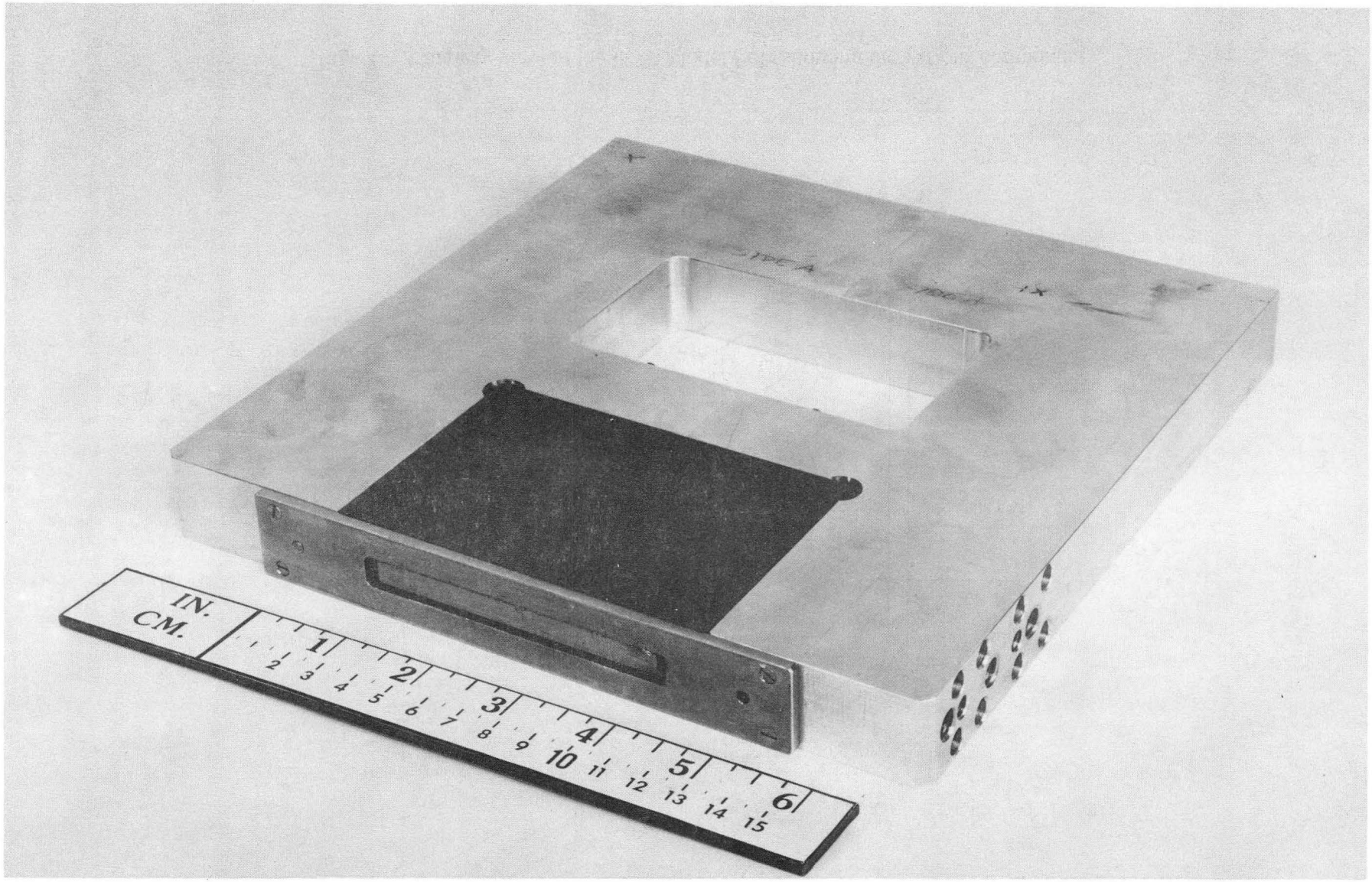

CBB 901-312

Fig. 3. Photograph of the pole keeper for the U5.0 Model Pole

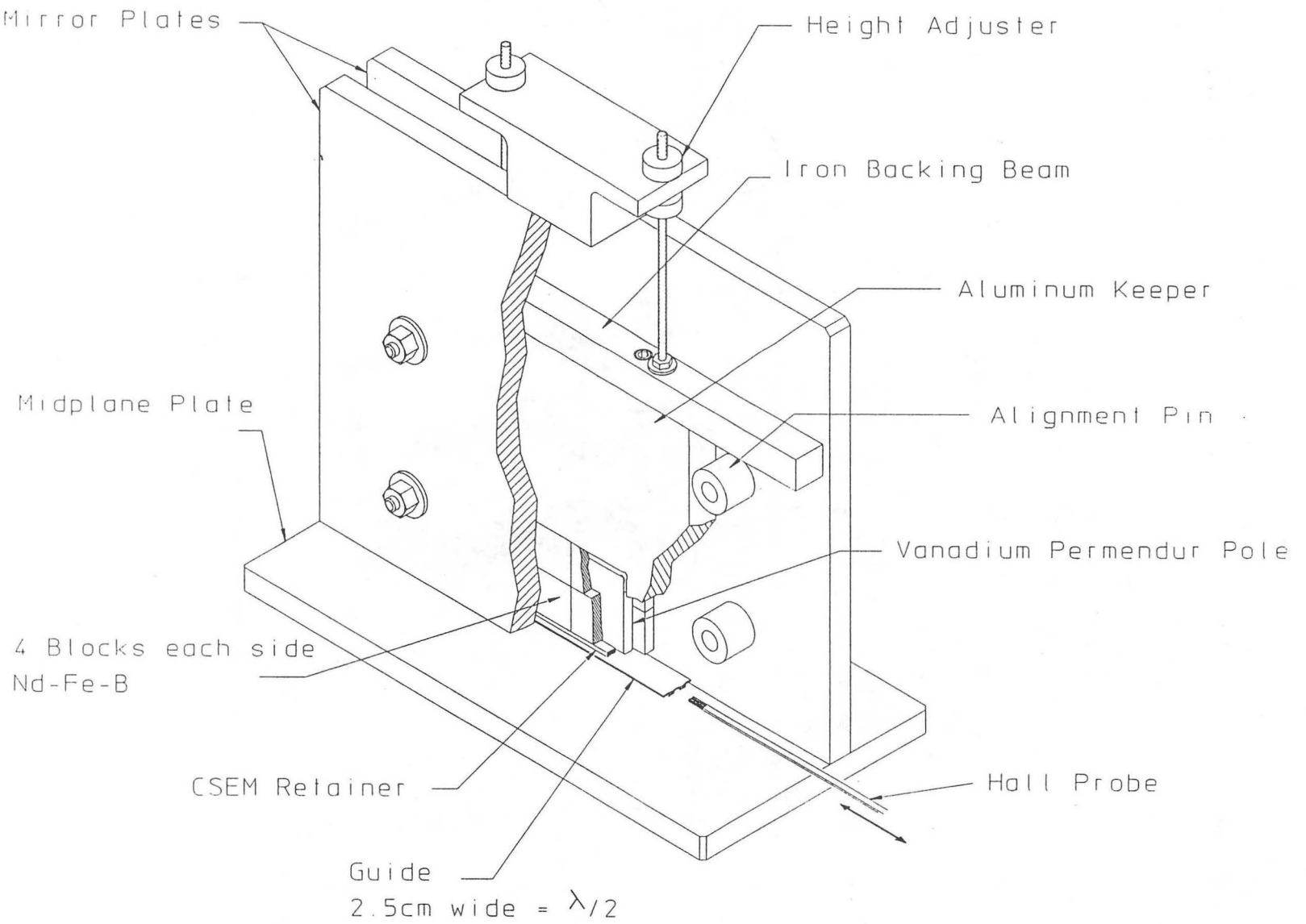

Fig. 2. Cutaway view of the U5.9 Model Pole showing the various components.

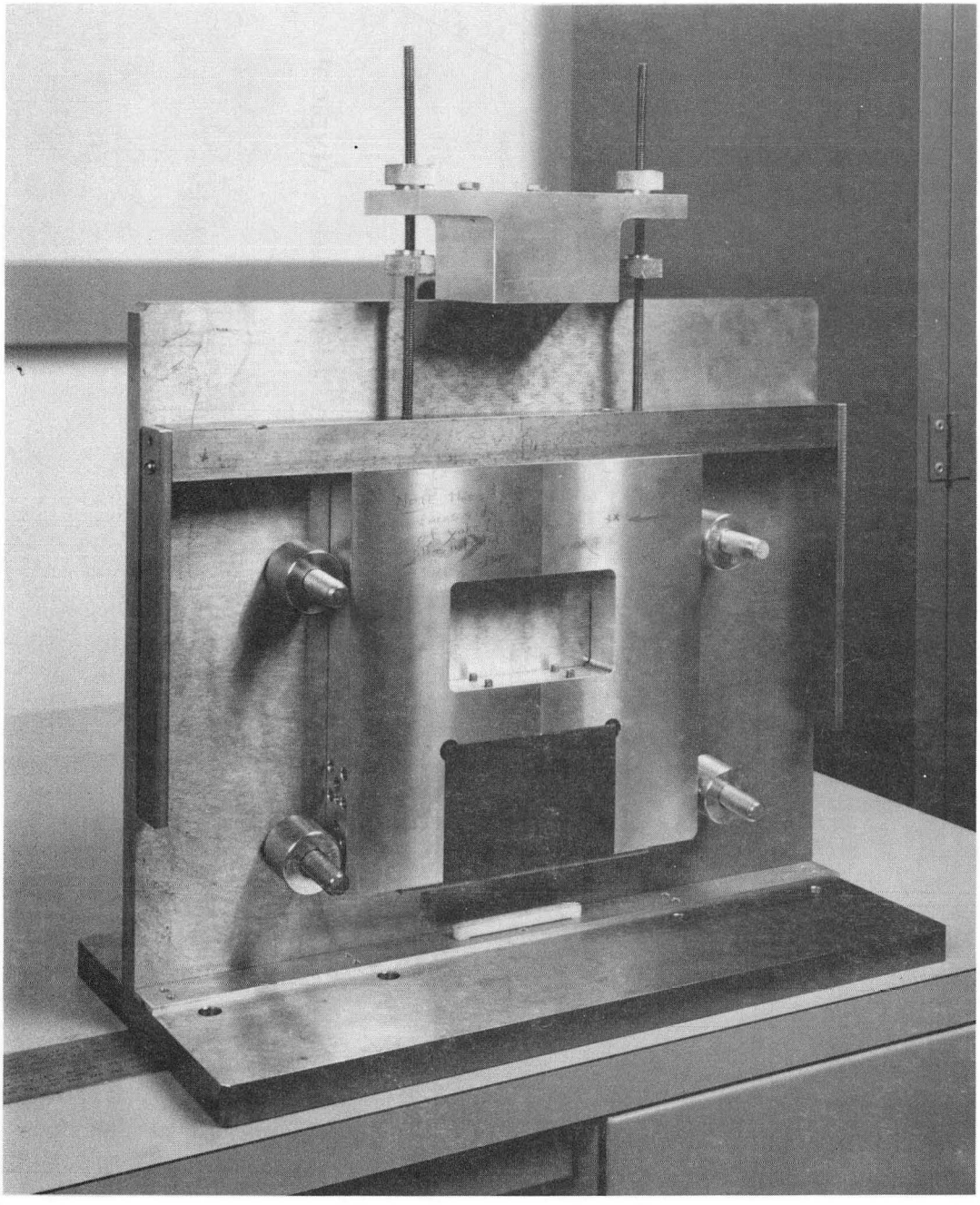

CBB 901-409

Fig. 1. Photograph of the U5.0 Model Pole.

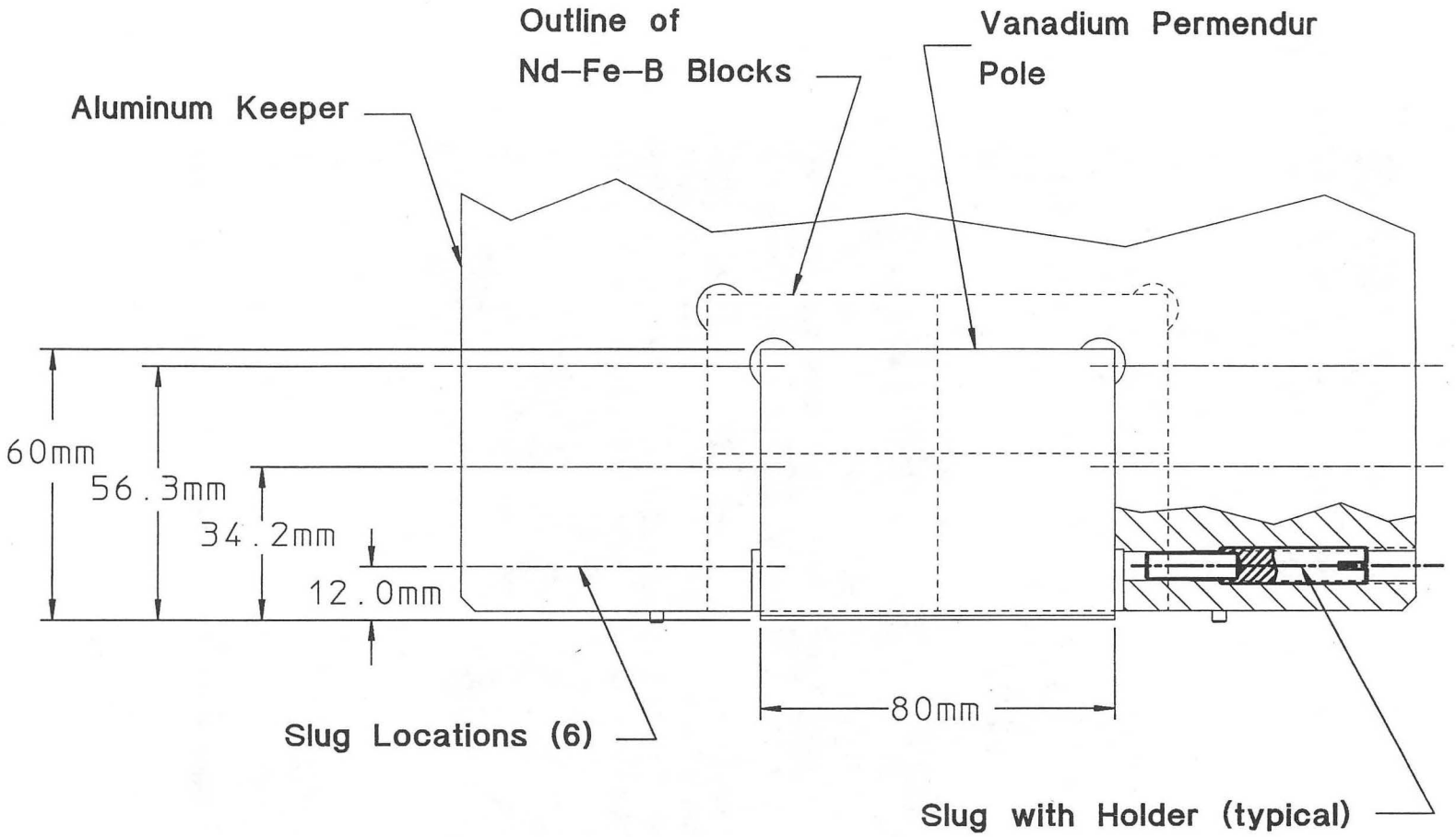

Fig. 4. Details of the of the CSEM and Vanadium permendur for the U5.0 Model Pole.

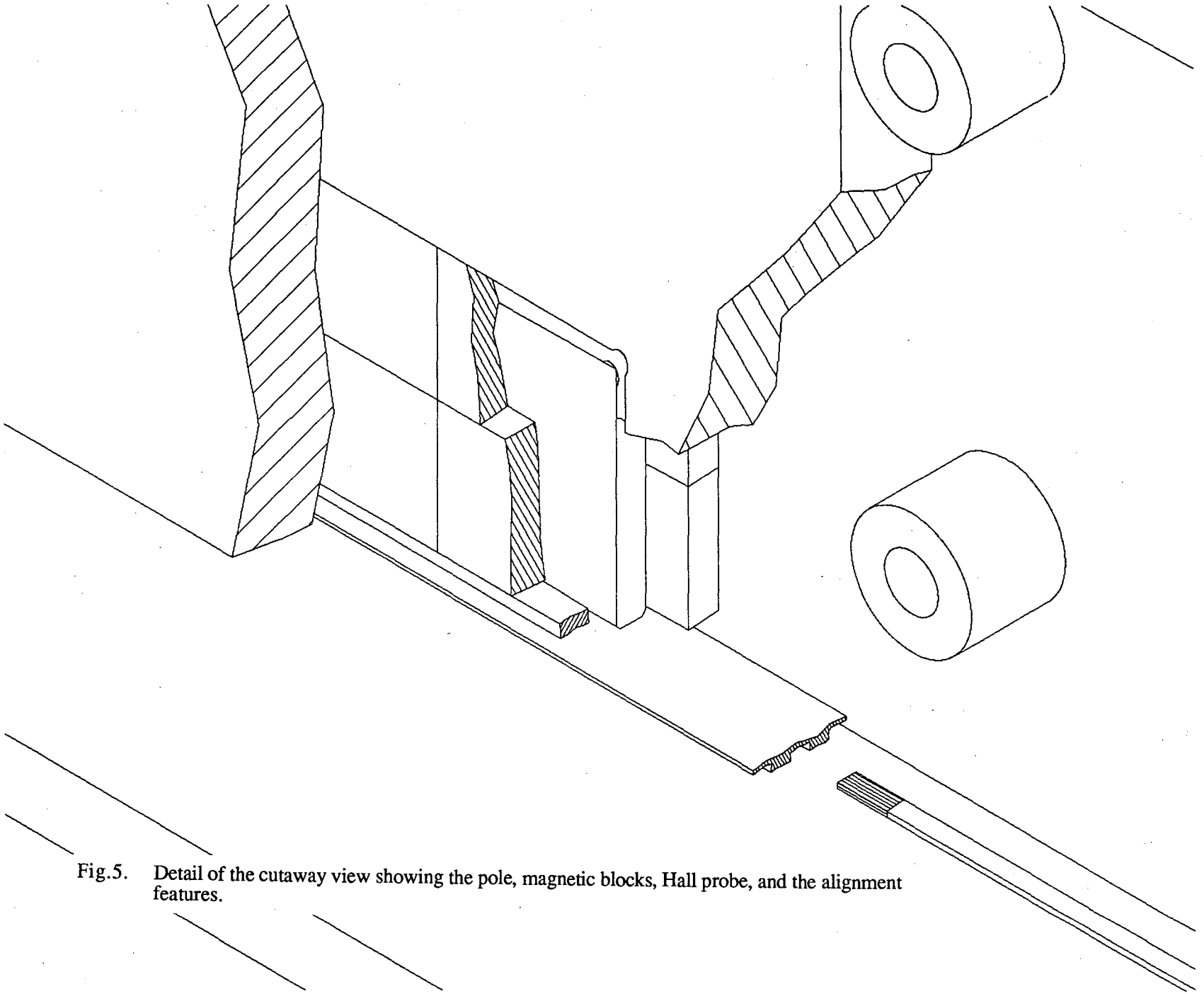

Fig.5. Detail of the cutaway view showing the pole, magnetic blocks, Hall probe, and the alignment features.

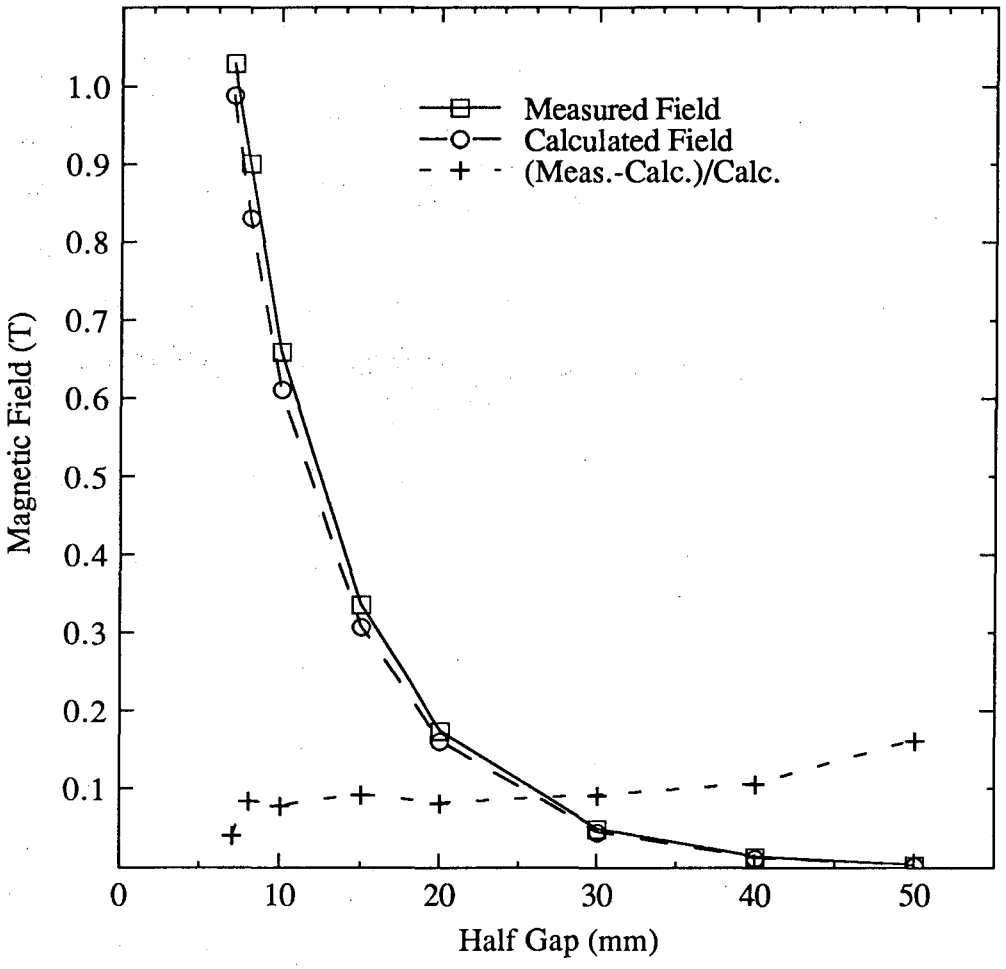

Fig. 6. A comparison of measured and calculated peak fields for the U5.0 model as a function of half gap.

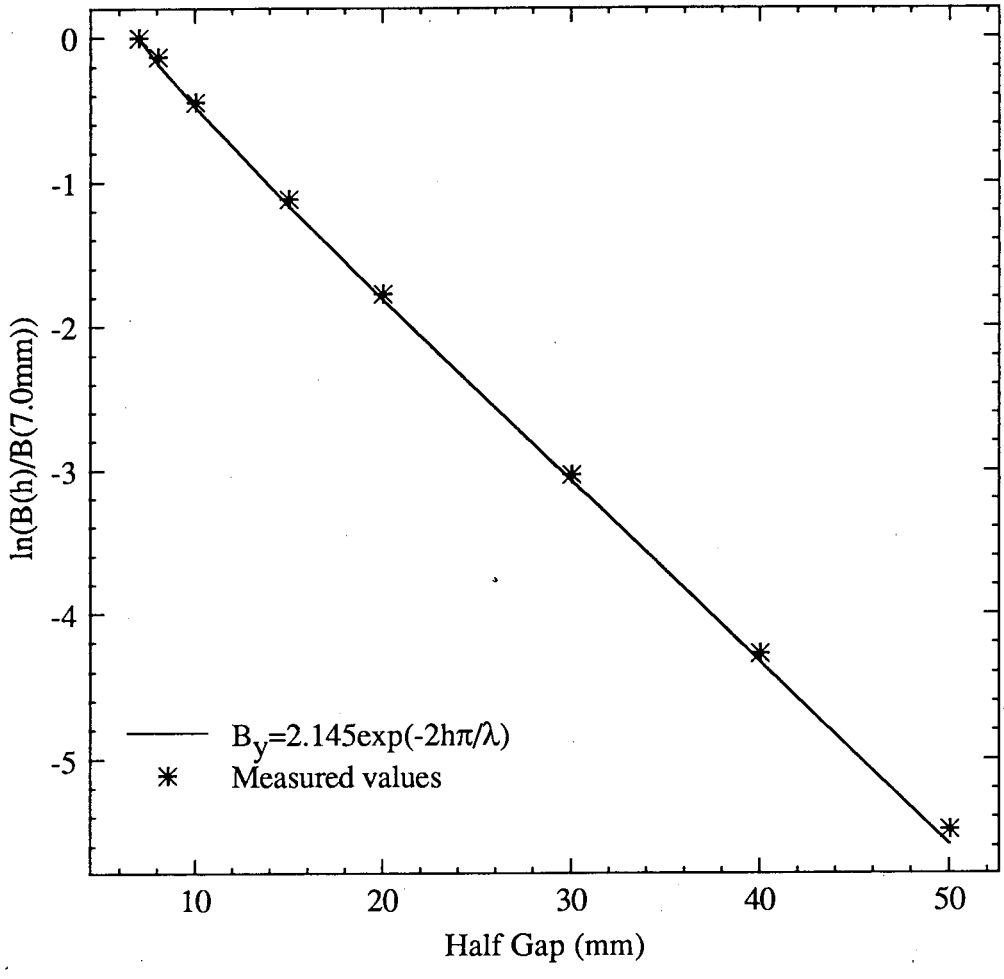

Fig. 7. Measured gap dependence of the peak field on a logarithmic scale.

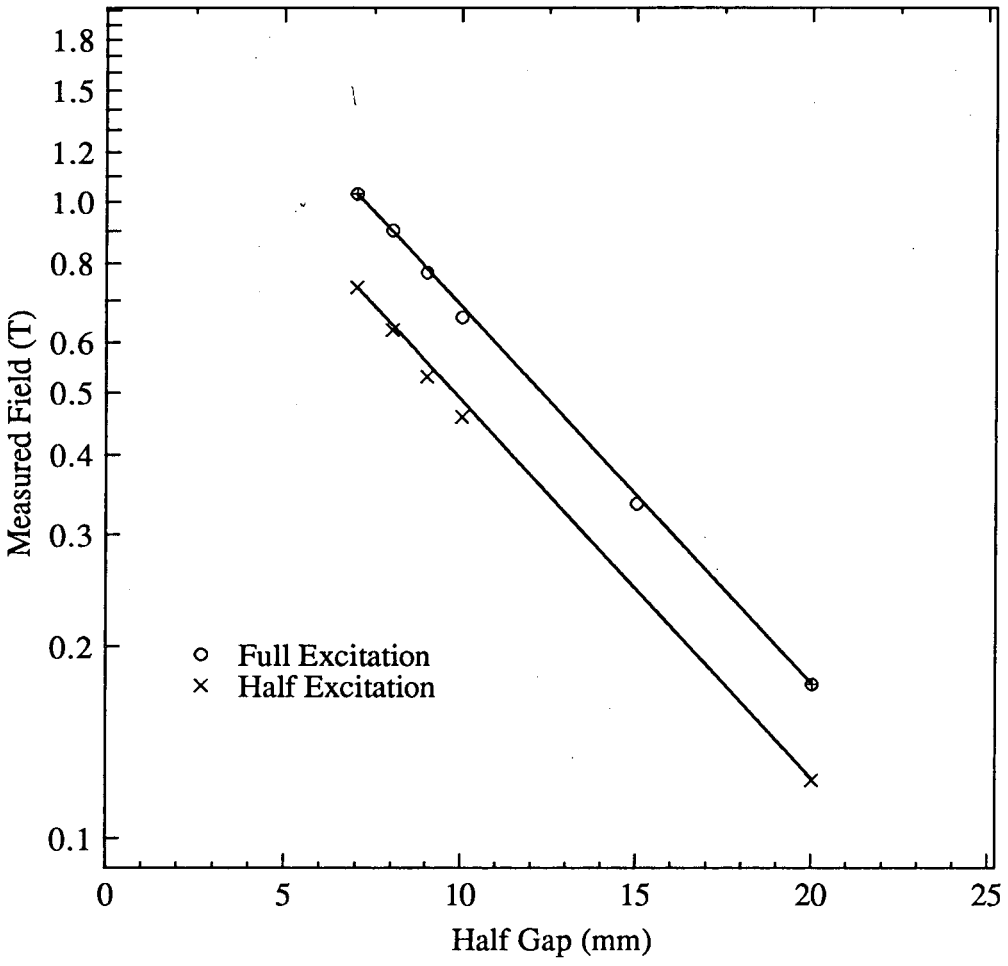

Fig. 8. A comparison of the peak field as a function of half gap for full and half energization of the pole. The straight lines simply connect the first and last points.

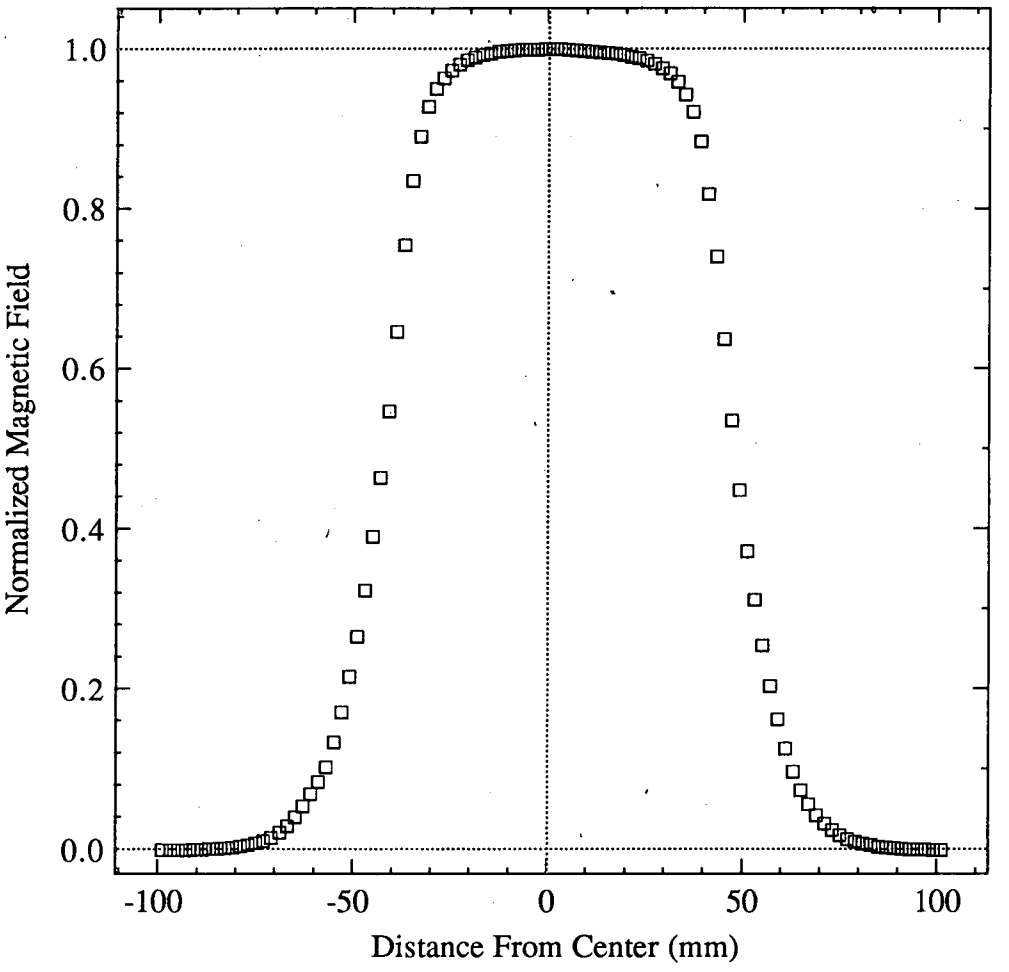

Fig. 9. Transverse field distribution for 7.0 mm half gap, maximum field is 1.029 T

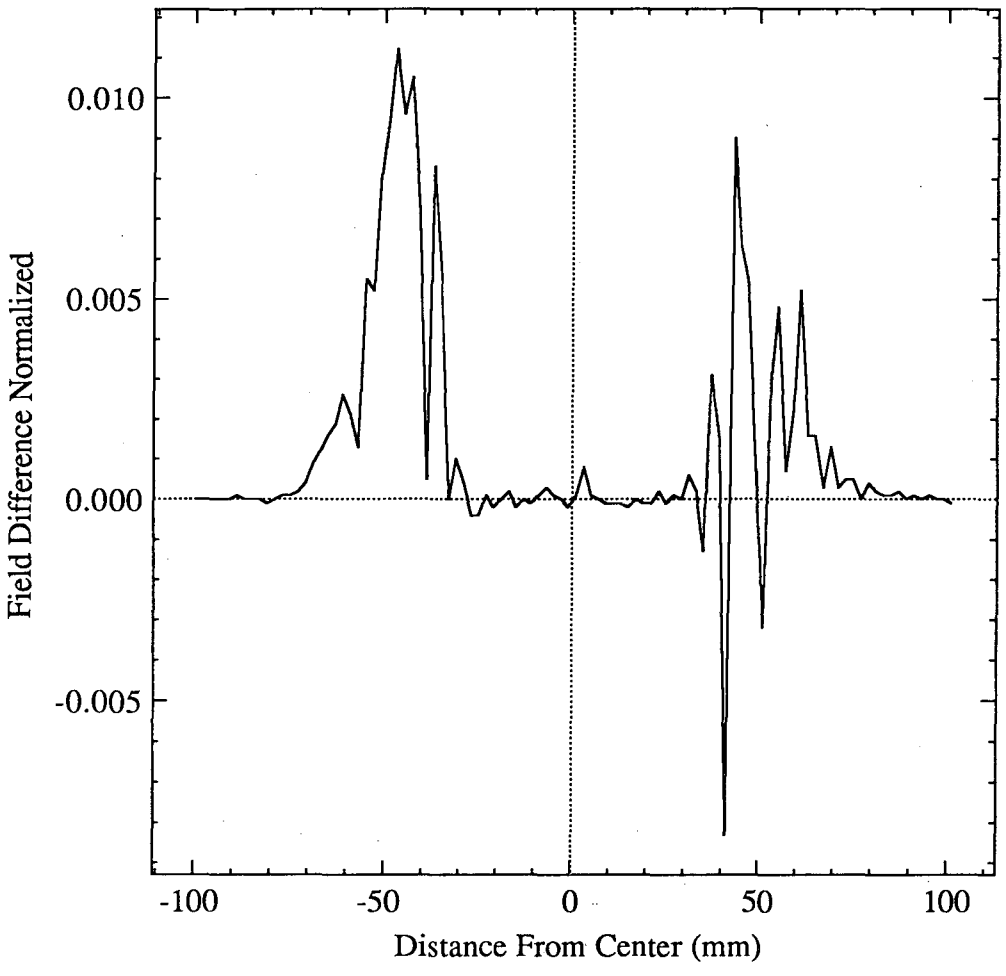

Fig. 10. Difference of two scans at 0.7 cm half gap showing repeatability of the field scan.

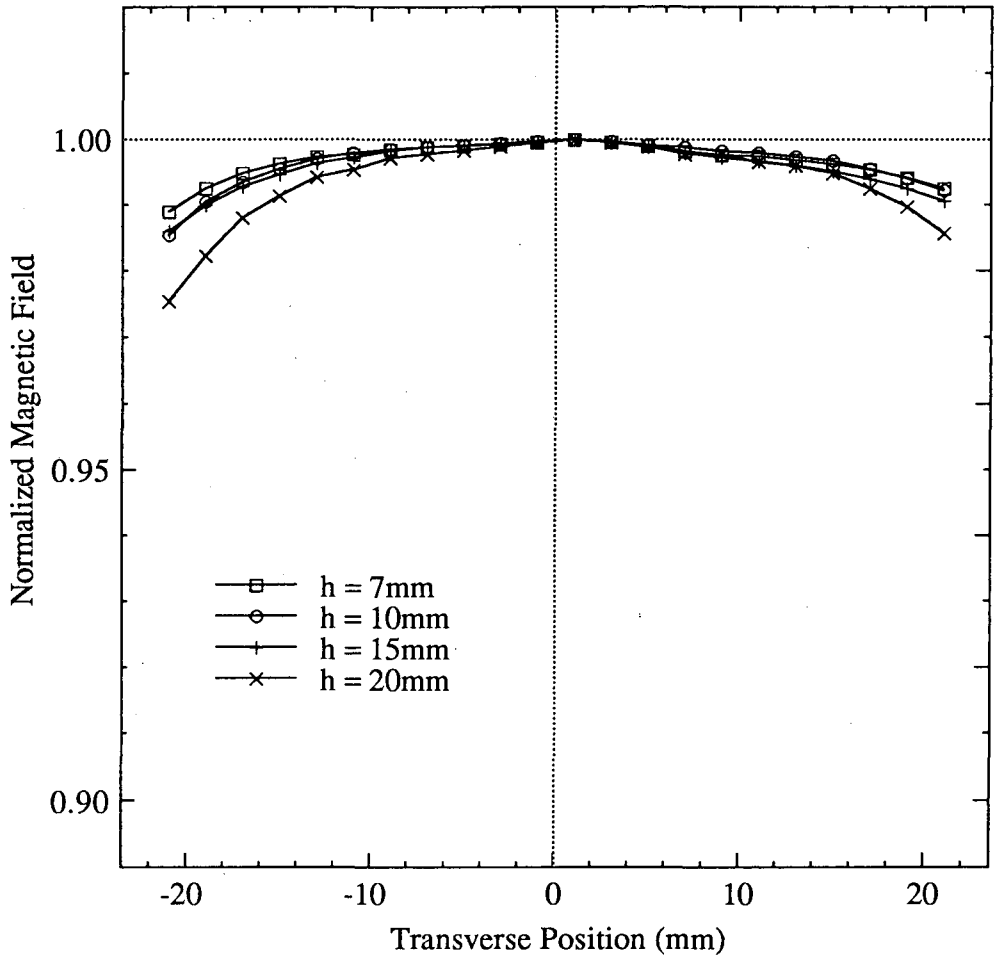

Fig. 11. Normalized field variation as a function of transverse position.

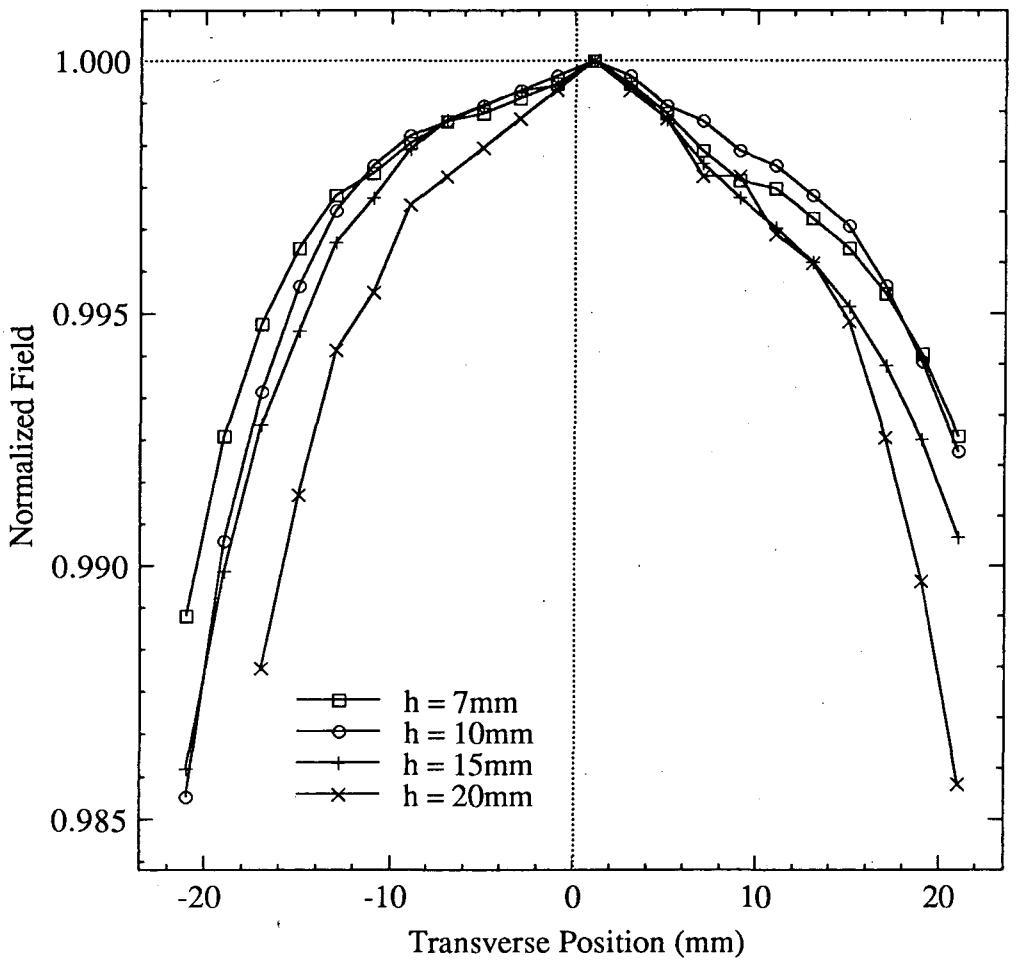

Fig. 12 Normalized field variation as a function of transverse position.

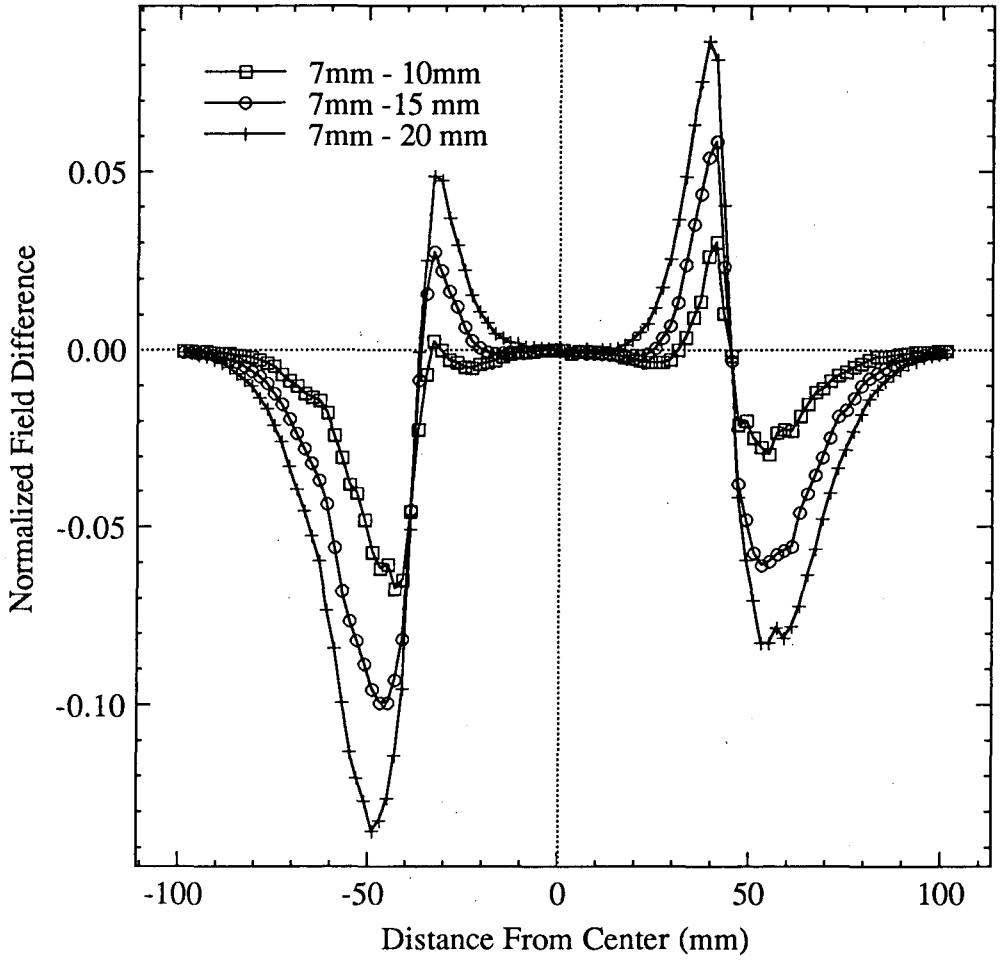

Fig.13. Plot of the difference in the normalized fields for various gaps.

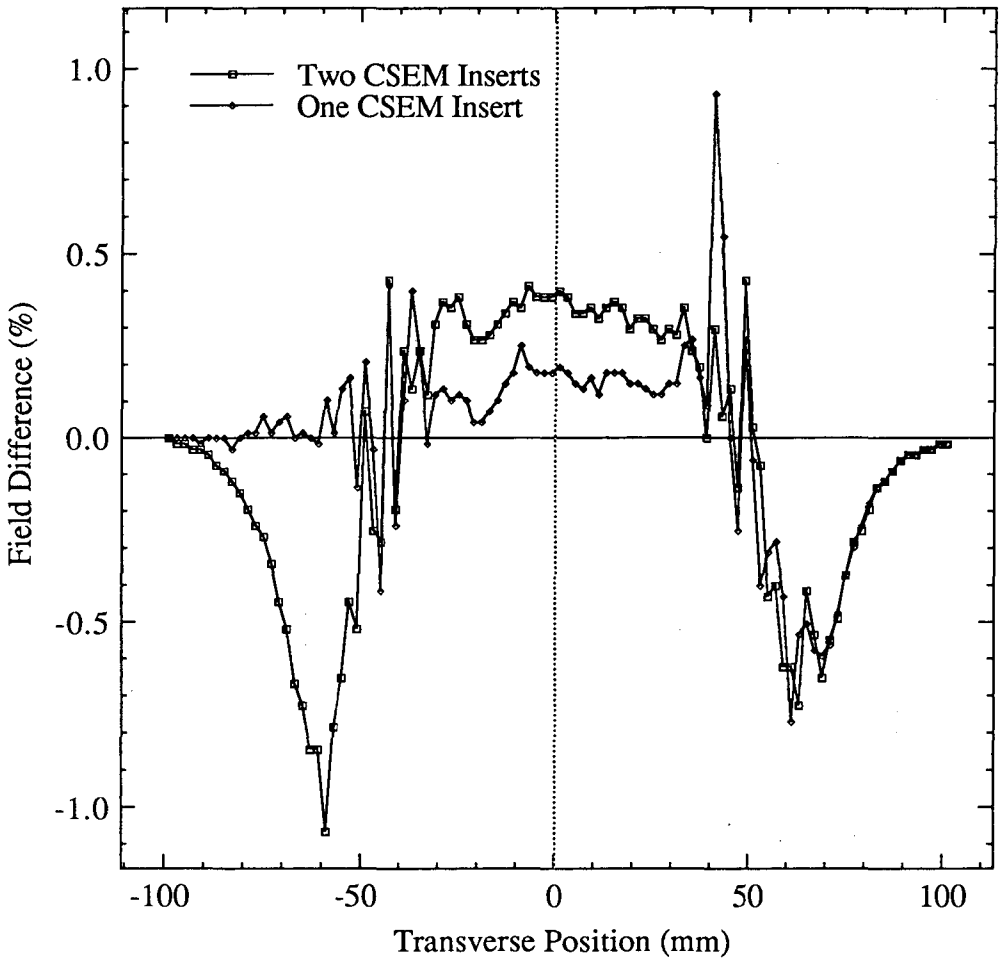

Fig. 14. Change in the field due to CSEM inserts for a 7 mm half gap.

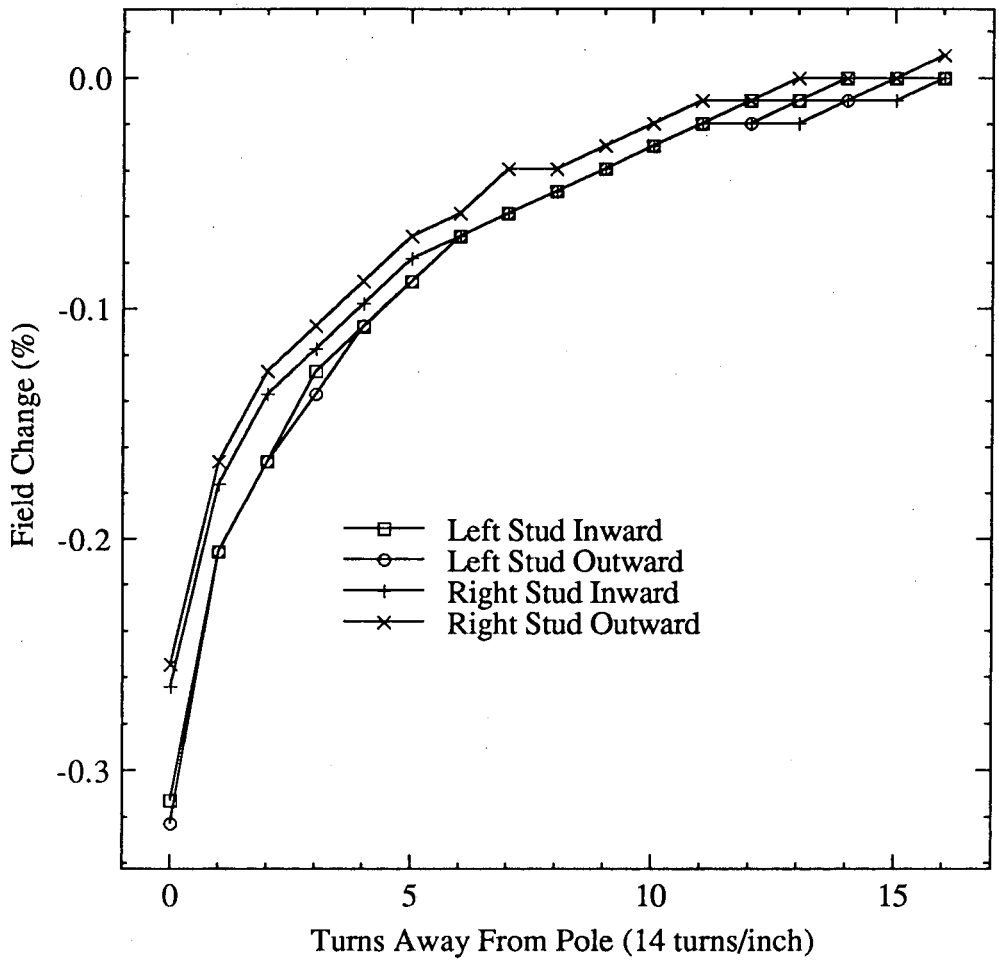

Fig. 15. Variation in peak field for different positions of the CSEM inserts.

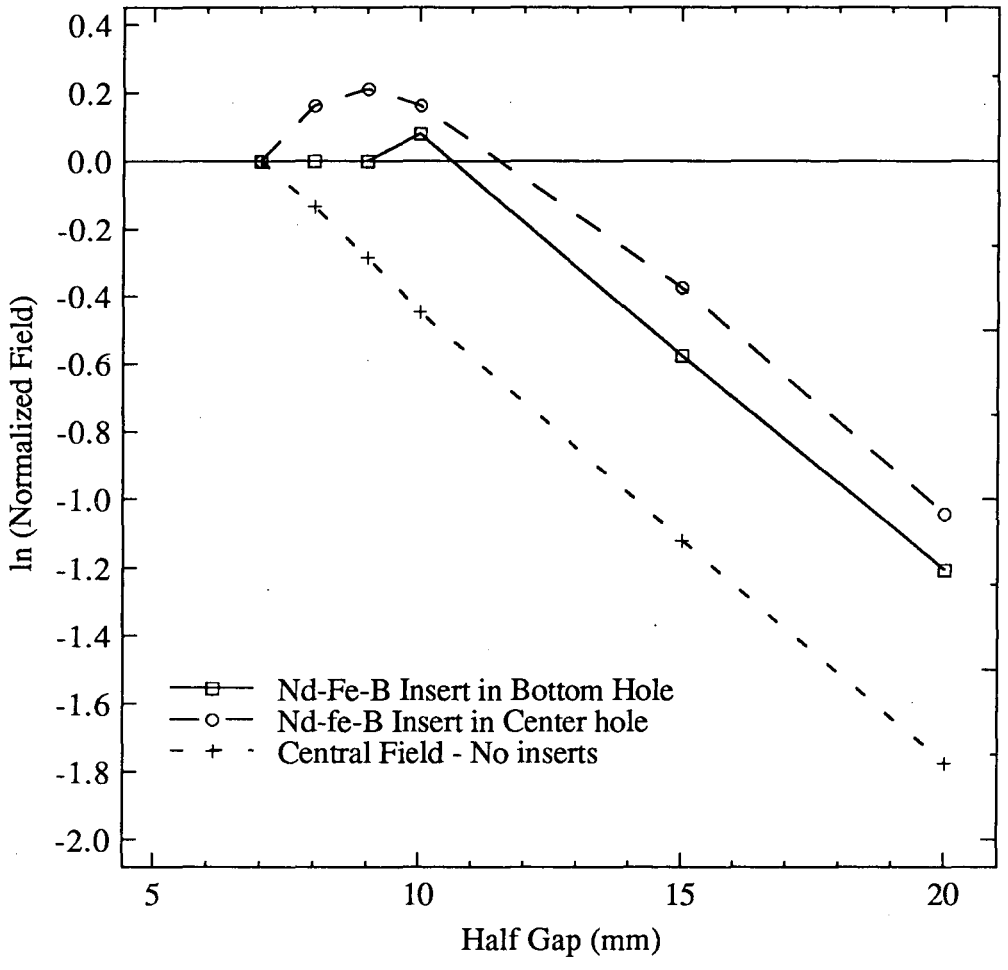

Fig. 16. Change in field as a function of half gap for the case of no inserts and for CSEM inserts in the bottom and middle positions.

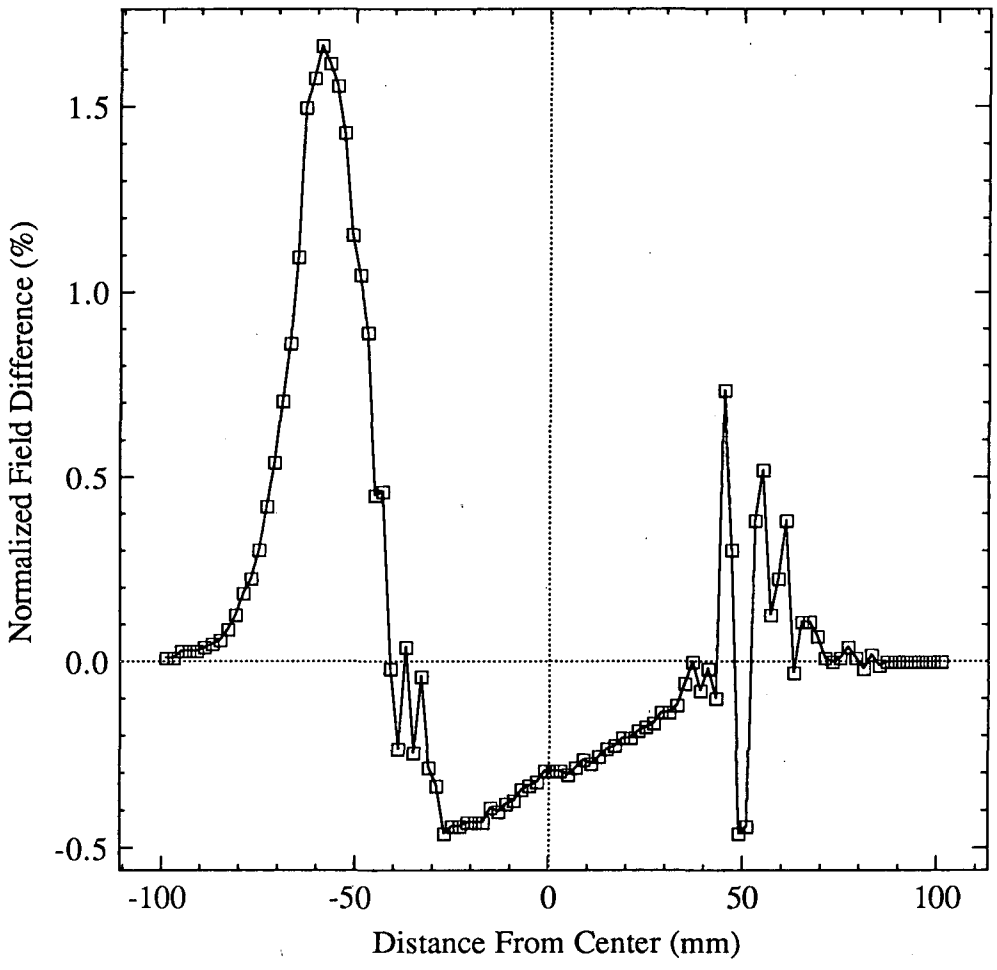

Fig. 17. Variation in normalized field for a 0.7 cm half gap due to an iron insert in the bottom position on one side. Note that the tilt of the field may be an indication of saturation.

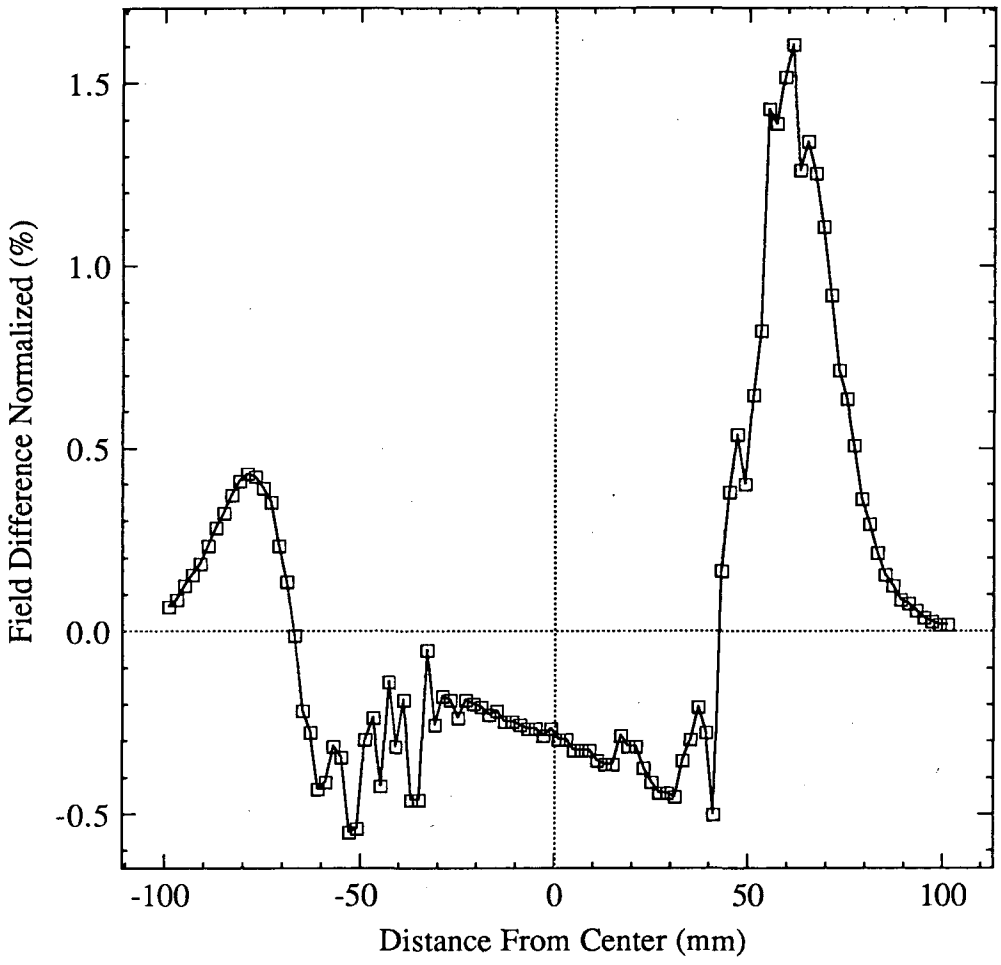

Fig. 18. Variation in normalized field for a 0.7 cm half gap due to an iron insert at the bottom position on the other side. Note that the tilt of the field may be an indication of saturation.

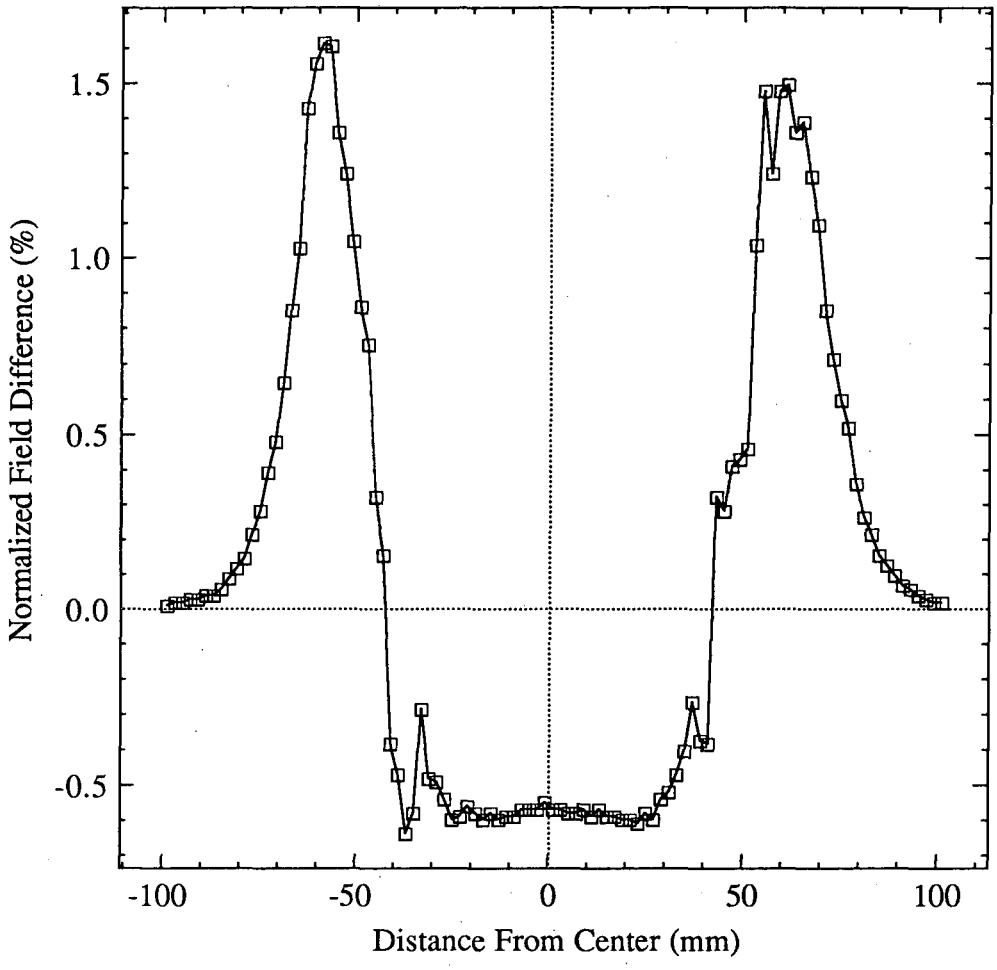

Fig. 19. Variation in normalized field for a 0.7 cm half gap due to two iron inserts at the bottom position.

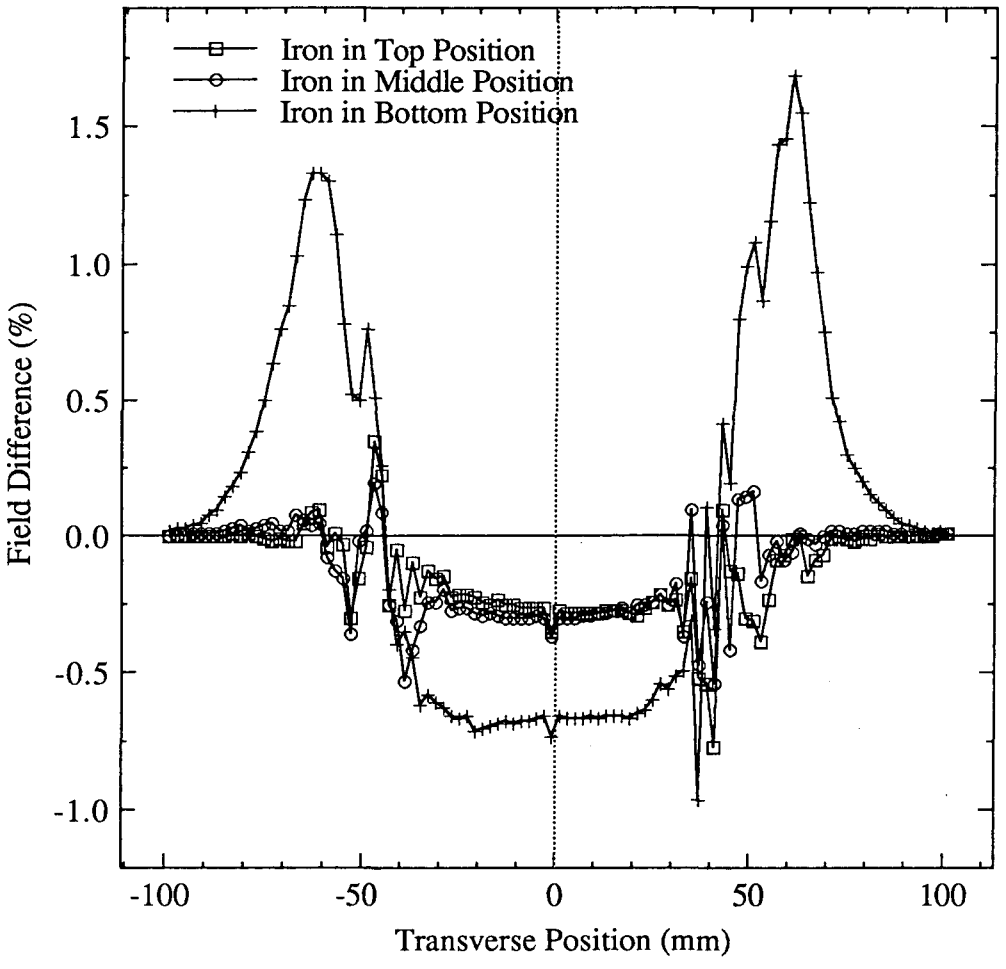

Fig. 20. Variation due to slugs in different positions at 0.7 cm half gap.

LAWRENCE BERKELEY LABORATORY
UNIVERSITY OF CALIFORNIA
INFORMATION RESOURCES DEPARTMENT
BERKELEY, CALIFORNIA 94720